ADEPT - A THIN-HAUL AIRCRAFT DESIGN CONCEPT

K. Poch, L. Hennies, S. Tarner, J. Belflower, J. Spittel, A. Graf, N. Schneiders, C. Klein
M. vom Schemm, F. Breer, M. Foery
Institut of Aerospace Systems, RWTH Aachen University
Wuellnerstrasse 7, 52062 Aachen, Germany

Abstract

The *Aachen Distributed Electric Propulsion Transporter* (*aDEPt*) presents a versatile aircraft concept that offers an efficient and cost-effective transport model for connecting remote towns or small cities to larger central hubs in metropolitan areas. Key design features derived from requirements set by the current market demands include a hybrid-electric powertrain, distributed electric propulsion systems, a morphing trailing edge as well as a practical cabin conversion and loading concept. The aircraft excels in terms of life cycle costs through optimized operation models, low noise emissions and high efficiency through the given propulsion system when compared to other thin-haul aircraft. Initial calculations, without considering autonomous flight, show that the *aDEPt* is 30.2%, 33.3% and 46.6% cheaper to operate than the P2012, C402, and PC12, respectively. This is, in part, due to the *aDEPt*'s capability of flying a fully electric 125 NM mission, which significantly reduces operating costs and emissions. The concept is designed for a maximum range of 350 NM with a cruise speed of 250 knots. Additionally the *aDEPt*'s avionics configuration allows for autonomous operations, making it a sustainable aircraft design for the coming years of aircraft operations.

Keywords Distributed Electric Propulsion, Hybrid-Electric Powertrain, Thin-Haul Market, Morphing Wing, Cabin Conversion Concept

1. INTRODUCTION AND MARKET ANALYSIS

Metropolitan areas of the world are commonly characterized as hubs of intermodal transport and by a strong economy. While the total world population living in metropolitan areas has superceded 50% as of 2007, a significant portion of the world population still lives in remote regions with limited access to various means of transport [1, 2, 3]. In this context, air transportation becomes more important for the trade of commercial goods, human mobility and economic development [4].

Airlines such as *Cape Air* (CA), America's largest commuter airline, are the vital link for rural communities to connect to larger hubs. In 2016, however, about half of CA's missions were subsidized by the *Essential Air Service* (EAS) program, as otherwise they would not be economically viable [5].

This is rooted in the economic challenges of thin-haul air travel. The connection of remote regions to the next airport is characterised by short and inconsistently frequented routes, which make scheduled air service more difficult and increase *Operating Costs* (OC) disproportionately. For example, none of CA's routes exceeds 225 NM, two thirds of the flown routes are even shorter than 100 NM (see Figure 1) [5]. Nevertheless, CA's business model of non-stop, low-fare service in smaller aircraft consistently attracts more passengers, which underlines the increasing demand in this segment of air travel [6].

However, none of the currently available 9-seater aircraft, like the widely used Pilatus PC-12 and Cessna 402 are optimized for the thin-haul market, which is especially evident in their excessive range capabilities. Additionally, many rural communities can be found in ecologically challenging areas that place additional demands on an aircraft, such as operating on water, under icing conditions or from very short and not paved runways. Due to the nature of this routes, CA and other commuter airlines insist on operating multi-engine aircraft in the future to decrease error-proneness [6].

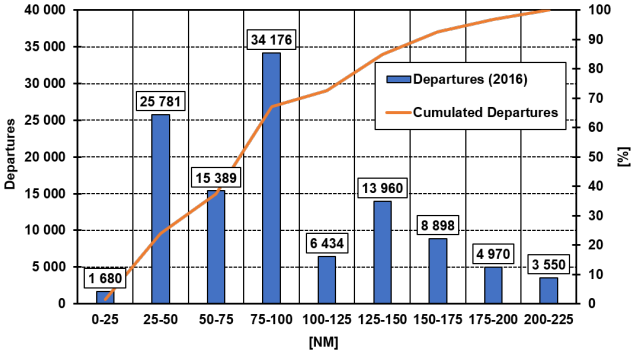

Figure 1: Route distribution of CA in 2016 based on [5]

In addition to non-optimized aircraft, the burgeoning shortage of qualified pilots also prevents commuter airlines from growing further into the market and thus from integrat-

ing more communities into the air traffic network [6]. By promoting increasingly autonomous air traffic this problem can be adressed. Furthermore, fully autonomous, ground-monitored flights offer great potential for reducing OC and error-proneness. By initially limiting autonomous flight missions to cargo missions the technology can be integrated into the market until a certain level of customer confidence is reached. This, however, places additional requirements on an aircraft, since an efficient cargo operation requires a sensible conversion and loading concept.

2. DESIGN SELECTION

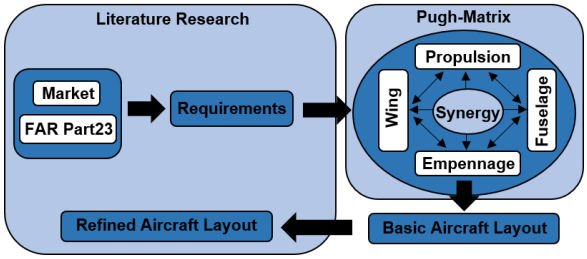

Figure 2: Methodology of the selection process

Figure 2 shows the overall schematic procedure conducted in this work.

2.1. Basic Considerations

In order to determine a feasible concept, the requirements specified by the market have to be derived first. Based on those requirements the figures of merit weight, complexity, flexibility/versatility, operating costs, error-proneness, sustainability and viability are chosen. A Pugh-Matrix is created and applied to the components propulsion, fuselage, wing and empennage to evaluate the strengths and weaknesses of each design. The values and weight factors are determined by the design team supported by additional literature.

A hybrid-electric powertrain architecture is chosen over a turbo-electric or full-electric approach since it offers versatility as well as OC reduction while less error-prone and with a much smaller weight penalty than a full-electric powertrain and no shortcomings in terms of OC and error-proneness when compared to the turboelectric approach. By further taking synergy effects into account, distributed systems offer the best approach in implementing the aforementioned powertrain. Furthermore, a high wing design is beneficial in regards to flexibility and versatility, since it is especially useful for cargo handling and poor ground conditions. Since the U.S restricts the airspeed to a maximum of 250 KIAS below 10 000 ft and a maximum flight time of 99 min is set as a requirement, a pressure cabin would be needed to cover a range of more than 350 NM. Nevertheless, an unpressurized fuselage is favored with the aim of minimizing weight, OC, complexity and error-proneness. With respect to the empennage the V- and U-tail reach the same score in regards to the chosen figures of merit. The V-tail is, however, favored to avoid negative influences by the prop wash of the wing mounted engines.

2.2. Refined Layout

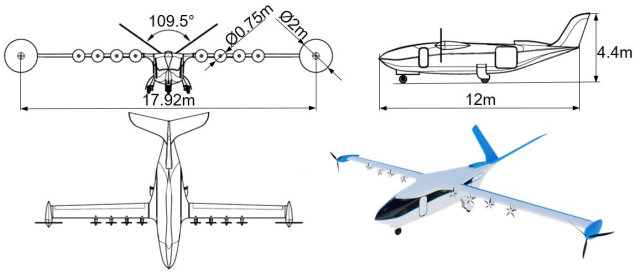

Figure 3: *aDEPt*

The *aDEPt* is designed with maximum flexibility and efficiency in mind for thin-haul operations. This includes hub-and-spoke missions as well as point-to-point operations in remote regions that would otherwise not be served by ground transportation. A *Distributed Electric Propulsion* (DEP) approach is chosen and extended by a sensible cabin conversion and loading concept, as well as a morphing wing to further optimize cruise performance.

Additional design freedom in regards to the fuselage can be achieved through the use of composite materials, which also reduce the structural weight.

In combination with an unswept wing the DEP approach allows operations on extremely short runways under poor ground conditions, which not only gives the *aDEPt* bush-plane-like capabilities, but also enables compatibility with future small airparks in otherwise dense suburban areas. Simultaneously, it increases the cruise efficiency as the increased maximum lift coefficient ($C_{L,max}$) allows a smaller sized wing while still fulfilling the stall speed requirement. The high wing loading also increases passenger comfort with regard to gusts. Furthermore, in combination with the hybrid-electric powertrain, the reliability is greatly increased. The wingtip propellers offer favorable interaction with the wingtip vortices and therefore decrease drag [7]. The *aDEPt* can fly missions up to 125 NM fully electric and up to 350 NM with a range extender. As battery technology advances, batteries can be gradually replaced by more powerful ones, thus increasing the electrical range, eventually rendering the *Turbo Generator* (TG) obsolete and therefore enforce sustainability. Additionally the *aDEPt* is equipped with the necessary technology for single pilot operations and autonomous cargo flights in all weather conditions. A functional fuselage design, which ensures passenger comfort as well as fast and simple cargo handling, completes the design.

3. DESIGN OVERVIEW

Beginning with the initial sizing, the component sizing has to be done iteratively to meet all performance requirements. Furthermore, some adjustments to the general design methodology have to be made to account for DEP. In order to manage the large amount of data and to be accountable for the numerous dependencies of individual design steps, the design is carried out with the help of numer-

ous programs authored by the design team.

3.1. Initial Sizing

A constraint analysis according to Gudmundsson is carried out in order to generate a starting point for the design of the hybrid-electric powertrain and wing [8].

As a first estimate an initial *Maximum Take-Off Weight* (MTOW) of 4 320 kg is assumed. This corresponds to the weight of the Tecnam P2012 surcharged by 20% to account for additional battery weight. Since the *aDEPt* does not have a pressurized cabin, the cruising altitude, cruise speed and climb rate are set to 8 000 ft, 250 KTAS and 1 200 ft/min, respectively. Furthermore, a *Take-Off* (T/O) run of 400 ft is chosen to achieve bush-plane-like flexibility and grant compatibility with future small airparks. In order to accomplish this, a stall speed of 50 knots is applied based on the data from NASA's SCEPTOR concept [9]. Figure 4 shows the corresponding constraint diagram.

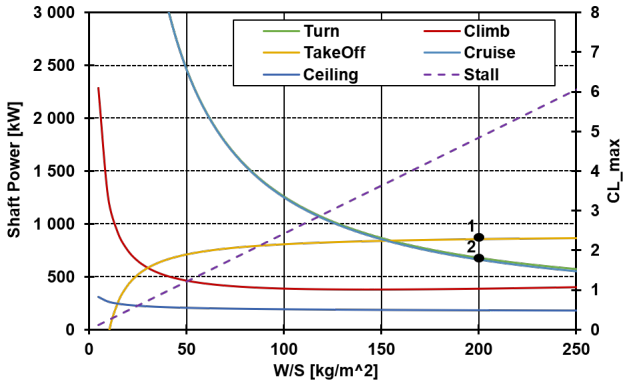

Figure 4: Constraint analysis of the *aDEPt*

Since DEP serves as an active high lift device, higher wing loading (W/S) is feasible compared to conventional aircraft. This increases both cruise efficiency and passenger comfort. A W/S of 200 kg/m^2 is selected taking into account structural and space-related reasons. Consequently a $C_{L,max}$ of 4.85 is required to meet the stall requirement. This serves as a constraint for the *High Lift Propeller* (HLP) design. To meet the power requirement a total shaft power of 860 kW is needed (point 1 in Figure 4). However, since the batteries can be used as a buffer for high energy demands, the TG can be scaled down. This leads to a second design point at 662 kW near the requirement for cruise and sustained turn.

3.2. Hybrid-electric Powertrain

The design of the hybrid-electric powertrain is determined by the designated mission profile, especially by the targeted electrical mission. Starting with the values from the initial sizing energy calculation has to be done iteratively in accordance with the optimization of the overall design ultimatly leading to the values seen in Table 1.

The *aDEPt* cruises at an altitude of 8 000 ft where only the *Cruise Propellers* (CP) have to be powered. To reduce drag the HLPs are folded back during all mission phases except

Mission Phase	Energy demand	
	Battery [kWh]	Fuel [kg]
Taxi out	6.34	-
T/O to 35 ft	2.71	-
Climb to FL80	58.97	-
Cruise	163.26	142.3*
Descent	9.80	-
Final Approach	22.01	-
Landing	1.23	-
Taxi in	6.09	-
Reserve Climb	-	23.90
Reserve Cruise	-	41.09
Reserve Holding	-	147.24
Reserve Landing	-	0.50
Reserve Taxi in	-	6.10
Avionics	16.22	17.87*

*For flights up to 350 NM

Table 1: Mission Data

T/O as well as at the beginning of climb and the end of approach where the *aDEPt* would stall without the lift increase provided by them. Because of the high *lift-to-drag ratio* (L/D) descent is possible with minimal energy consumption. During the final approach the HLPs are used to lower the stall speed while the *aDEPt* gradually decelerates. In this phase the CPs provide drag through windmilling or reverse thrust to enable deceleration even though the HLPs are at full power [10]. In case of a go-around an alternate airport can be reached at a distance of 100 NM. Additionally, a final reserve of 45 min (holding) is provided.

3.2.1 System Architecture

The *aDEPt* focuses on a high lift coefficient at low speeds to allow operation from short runways, while ensuring optimum L/D and maximum drive train efficiency. For this purpose, several electric drives similar to the *SCEPTOR* are used [11]. The engine sizing is carried out according to Stoll et. al. and results in the following motor configuration [12]:

- Two cruise motors with 267.5 kW power and a propeller diameter of 2.0 m
- Eight high lift motors with 55 kW power and a propeller diameter of 0.75 m

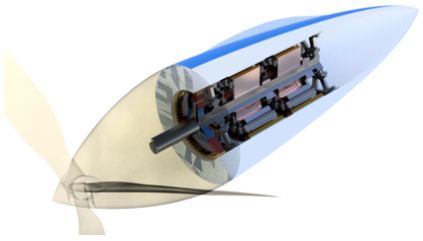

Figure 5: Double motor configuration

For the CPs a double motor configuration as depicted in Figure 5 is used to increase redundancy and decrease the loss of thrust in case of a motor failure [13].

The complete electrical system architecture features a redundant interconnection mode in which two independent controllers and three spatially separated battery packs are used. This guarantees reliability in the event of fire outbreak or electrical issues [14]. Figure 6 illustrates said architecture including the efficiencies of the individual components as proposed by literature [15].

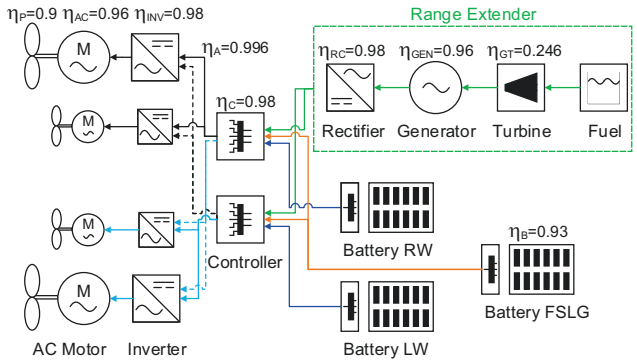

Figure 6: Powertrain architecture

3.2.2 Battery

A demanded design mission of 125 NM should be flown fully electric. This corresponds to about 80% of CA's total flights as well as 98% of their flights not subsidized by the EAS program in 2016 (see Figure 1) [5].

Based on literature a gravimetric energy density of 400 Wh/kg is assumed for the year 2025 [12]. Together with the required power per flight segment to fulfil the design mission and the efficiencies of the various components in the powertrain (see Figure 6), the required energy per flight segment can be obtained (see Table 1). The resulting battery data is listed in Table 2.

Data	Unit	Value
Gravimetric energy density	$[\frac{Wh}{kg}]$	400
Volumetric energy density	$[\frac{Wh}{l}]$	300
Total energy	$[kWh]$	315.07
Weight	$[kg]$	787.68
Volume	$[m^3]$	1.05

Table 2: Major battery data

The total energy requirement results in 315.07 kWh including a safety margin of 10% to consider possible perturbations during flight. In addition, Kreimeier cites a volumetric specific energy density of 300 Wh/liter, which results in a battery volume of 1050.24 liters (1.05 m^3) [14].

The batteries are located in the fuselage as well as in the inner parts of both wings. In case of short turnaround times the batteries in the fuselage can be replaced easily through the landing gear bay. The battery units in the wings are scaled in such a way that they can be fully charged with two 150 kW direct current chargers in an available turnaround time of about 30 min. A liquid cooling system is used in order to dissipate the generated heat during charging, which also arises at increased loads in flight [15].

3.2.3 Turbo Generator

Since the assumed energy density of batteries in the near future makes it infeasible to operate fully electric aircraft with short T/O capabilities like the *aDEPt* at typical commuter flight ranges, a TG powered by kerosene is installed in the aft to combat this issue.

The TG provides enough power to function as a range extender for all missions longer than 125 NM including the reserve mission in case of an aborted landing.

Since the batteries bridge the power difference between T/O and the remaining flight phases the TG can be operated close to its design point the whole flight. This drastically reduces kerosene consumption and emissions and enables significantly higher efficiencies. The placement of the TG incorporated in the aft and the use of a smaller gas turbine also greatly reduces noise levels. For reference the PT6A-41 is used. This gas turbine complies with the calculated power requirement. Additionally the PT6A-41 is one of the most common engines, which makes maintenance and servicing simple and inexpensive [16].

3.3. Fuselage and Cabin Design

The *aDEPt*'s fuselage and cabin design is characterized by a focus on versatility and adaptability to client requirements. Keeping low turnaround time requirements in mind, the chosen concept makes the cabin conversion between cargo and passenger missions possible without removing or adding any components at the local airport. Subsequently, this enables the *aDEPt* to fly point-to-point mission models varying freely between passenger and cargo missions versus solely hub-and-spoke missions.

3.3.1 Fuselage Sizing

The cabin dimensions are compared to the reference aircraft in the *aDEPt*'s design process to assure that realistic values are implemented. Using these dimensions and assuming sufficient space for the cabin floor, skin- and structure thickness and landing gear storage, a basic fuselage form is determined. Further refinement of the fuselage shape takes its aerodynamic properties into account. Junctions between the fuselage and wing are gradual, minimizing induced drag and designed with a geometry similar to a lifting body to optimize the incident flow at the empennage. In order to obtain an aerodynamic fuselage with sufficient cabin space for the comfortable transport of passengers and cargo, numerous simulations with different cross-sections over the fuselage length are carried out with *OpenFOAM*. The large, cargo compatible fuselage makes it possible to design the landing gear to retract into the fuselage to further reduce drag.

The seat design shown in Figure 7 is an adaptation of

Seymourpowell's Morph seating concept. This concept uses fabric made of high-tensile fibers stretched over retractable railings to adjust comfort and partitioning of the three-abreast seat bench. The adapted system offers the same high level of comfort, due to the adjustable design and hammock-like seating feel, while offering an excellent opportunity for minimizing seat-dimensions in a stowaway configuration [17, 8, 18].

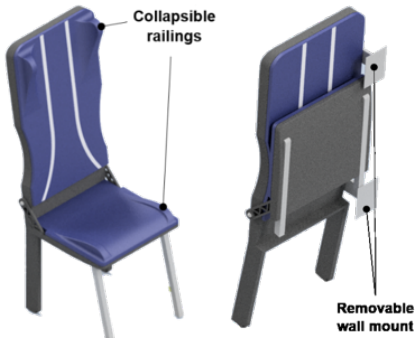

Figure 7: Seat design

Additionally, due to the collapsible seat volume, material weight is reduced in the seat design. The *aDEPt*'s seating system features a mounting port for a carrying hinge that eases the stowaway and set-up of the seats. The possibility of decoupling the hinge and seat gives the carrier the option of removing the seats between passenger and cargo missions to avoid dead weight during the flight. In this case, the lightweight and foldable design remain beneficial for the cabin conversion.

3.3.2 Cargo Configuration

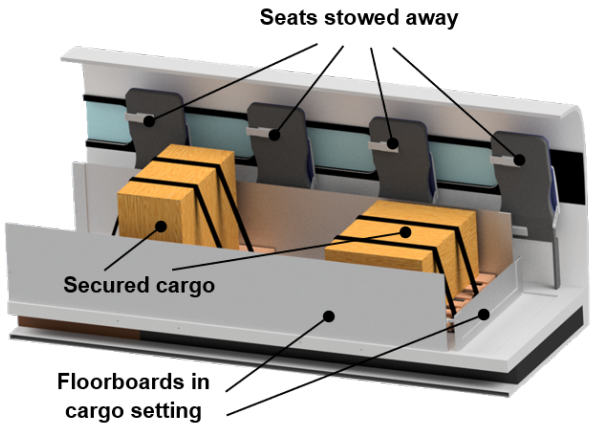

Figure 8: Cabin in cargo configuration

In the cargo configuration, the fuselage is designed to hold up to four standard GMA or EPAL2 pallets, or five EPAL1 pallets, on which the cargo load can be evenly distributed, as all three standards are widely used on the international market [19]. Designing around these standardized dimensions decreases turnaround times and OC during cargo missions compared to having a proprietary pallet system. This is because depalletizing and repalletizing cargo becomes unnecessary, though the use of plastic pallets is advised in order to save weight [20]. Furthermore, the cargo volume capacity of the *aDEPt* is estimated at 7.33 m^3, 6.36 m^3 of which can be directly loaded onto the pallets as constrained by the loading door. The crates can be secured atop the pallets once in the cabin to make use of the remaining space. The loaded pallets alone achieve a chargeable weight of 157 kg/m^3, improving on the volume capacity of the chargeable weight average of 167 kg/m^3 prescribed by the *International Air Transport Association* [21]. Using mail crates in the remaining space, for instance, further boosts the chargeable weight average of the volumetric cargo capacity to 136 kg/m^3.

The cargo cabin configuration is assembled by setting the seats in a stowaway position, turning the floorboards up in a 90° position and lastly setting the floor supports down that would otherwise provide an even load distribution on the sandwich-structure floor boards. This reveals the roller system below, on which the cargo pallets are loaded, positioned, and secured via restraints between the rollers.

3.4. Morphing Wing

The *aDEPt's Trailing Edge* (TE) movement is realized by electro-mechanical actuators in combination with wire rope hoists, as tested by NASA on a Gulfstream III in 2015 [22]. As shown in Table 3 a gap between flap and wing influences the lift coefficient and L/D-value. In order to fly more efficiently a higher L/D-ratio is desirable. The smooth transition between wing and flap reduces the friction of the airflow compared to conventional flap systems, thus increasing the L/D (see Figure 10).

Gap	C_L	C_D	L/D	C_{Lmax}
1% cord length	0.26	0.023	11.13	1.97
0% cord length	0.26	0.018	14.06	1.91

Table 3: Influence of a flap gap at 20° flap angle

The TE incorporates eight multifunctional flaps (four on each side). By exploiting the high adjustment rate, this system combines high-lift devices and ailerons. Due to the large effected area and an independent control of the individual control surfaces the high lift capabilities of this design are suitable for short T/O. Additionally, a steeper and slower approach can be guaranteed, which shortens the landing distance. The low response times of the electrically operated morphing system allows to respond to spontaneous aerodynamic loads like wind shear and gusts and can be controlled to reduce overall material strain. Additionally, it allows the steering of wind conditions to improve passenger comfort [23].

3.4.1 Performance Analysis

The GAW-1 and GAW-2 airfoils are developed to meet all requirements made on a wing in general aviation. These airfoils combine high lift with low drag, which is important for

short T/O distances and efficient cruise conditions. Therefore both airfoils are analysed with focus on cruise, landing and T/O performance as well as space for system integration. In order to calculate the performance of the morphing wing under various conditions the airfoils are morphed with the help of a self-written *Python* script by rotating the mean camber line at 70% relative cord length in steps of 0.1° (see Figure 9). The resulting end position and local gradient of the profile line at 70% cord length are used to determine the morphed geometry.

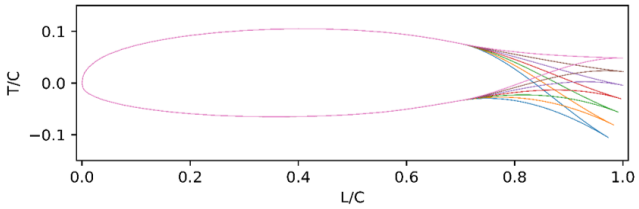

Figure 9: Example airfoil GAW-1 morphed in 5° steps

The aerodynamic characteristics are calculated using *XFOIL* [24]. In Figure 10 the wing performance can be seen for a range of C_L values for three different cases. The blue curve (Morphed Profiles) connects the best L/D values achieved at certain C_L-values with the GAW-1 and GAW-2 airfoils with thickness scaling applied to values between 15% and 19%. If one of the two GAW-1 curves intersects or coincides with the morphed profile curve, this implies that the given airfoil has the best L/D for this C_L-value.

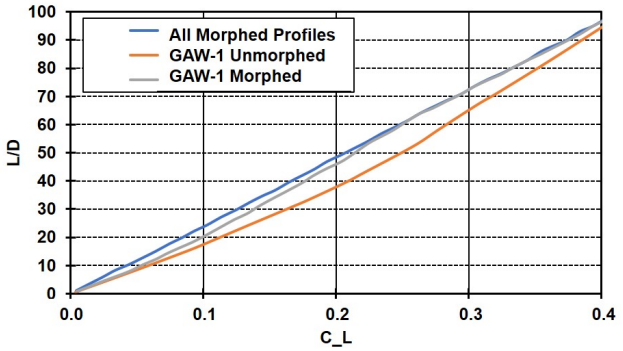

Figure 10: L/D over C_L (Re = 8.32e6 M = 0.39)

The chosen speed, altitude and wing loading yield a required C_L-value in cruise of 0.2638. As seen in Figure 10 the GAW-1 with a standard thickness of 17% is the best airfoil under cruise conditions. It offers a high $C_{L,max}$ ($C_{L,max}$ = 2.47) value with flaps in a 40° position, decent stall speed and high performance during T/O and landing. Furthermore, it provides enough space within the wings for structural parts, batteries and cooling- and de-icing-systems.

Regardless of the current aircraft weight or speed the angle of attack can be kept constant during cruise. Therefore, the fuselage creates the minimum drag possible and the L/D-ratio is optimal during the entire flight. For the design passenger mission this results in an profile L/D of 64.5, compared to a non-morphed profile L/D of 53.7.

3.4.2 Synergy with DEP

The HLPs are installed upstream to the leading edge of the wing increasing the incident flow velocity and hence dynamic pressure at the wing due to the propeller induced velocity. This results in a significant lift increase during low velocity flight, especially during T/O and landing. The CFD simulations conducted with *OpenFOAM* indicate a C_L increase of 2.6 for a stall-speed of 25 m/s. This is in line with Stoll's momentum theory-based approximation [12]. Therefore the blown airfoil achieves a $C_{L,max}$ of 5.6 with a 20° flap angle.

3.5. Empennage

To obtain a V-Tail configuration the horizontal (H) and vertical (S) stabilizer are geometrically designed separately. The corresponding design case for the horizontal stabilizer is the static longitudinal stability at T/O (see Equation 1) [25, 26].

(1)
$$\frac{S_H}{S} \geq \frac{C_{m0FR,max} + \frac{x_{CGV} - x_N}{MAC} C_{LFR,max} - V_T C_{T,max}}{C_{LH,min} \eta_H \frac{r_H}{MAC}}$$

The design case for the vertical stabilizer is directional stability in the event of one-sided damage to the cruise propeller during T/O and a crosswind of $0.2V_S$ (FAR Part 23). If the sensors detect an error in a CP-system, the computer automatically adjusts the propeller pitch angle of the CP on the opposite side to idle speed, brakes it to a standstill and finally switches it off. This prevents a dangerous influence of the long lever arm. The HLPs have enough thrust to continue the T/O process. In cruise flight, the failure of a CP can be partly compensated by the use of the HLPs on the same side and can therefore be assessed as uncritical compared to T/O.

For a laterally stable aircraft the yaw rate caused by sideslip angle β must be positive ($C_{n\beta} \geq 0$) (see Equation 2) [23].

(2)
$$C_{n\beta} = C_{n\beta,fslg}\beta + C_{n\beta,wing}\beta + \Lambda - \frac{\Delta T}{qS}\bar{y_t}$$
$$\Lambda = \eta_S \frac{\delta\beta_S}{\delta\beta} \beta_{eff} \frac{S_S}{S} C_{Y\beta,S} \left(\bar{X_S} - \bar{X_{CG}}\right)$$

Subsequently the resulting tail surfaces, which are needed to ensure stability, are combined. Table 4 summarizes the geometric data of the V-Tail.

Geometry	Unit	Value
Area	$[m^2]$	8.582
Aspect Ratio	[-]	6.0
Taper Ratio	[-]	0.6
Halfspan	[m]	3.588
Opening Angle	[°]	109.458
Leading edge sweep	[°]	20
Relative rudder depth	[-]	0.3

Table 4: Geometry of the V-Tail

3.6. Weight and Balance

To estimate the aircraft mass, empirical formulas according to Raymer and NASA's *Flight Optimization System* (FLOPS), as well as specific power ratios for the hybrid-electric powertrain proposed by literature are used [15, 27, 28]. Since no public component mass distributions exist for the reference aircraft, the developed model is verified based on the *Manufacturer's Empty Weight* (MEW) given in the literature to ensure that the implemented model does not deviate further from the MEW than the individual models of the authors.

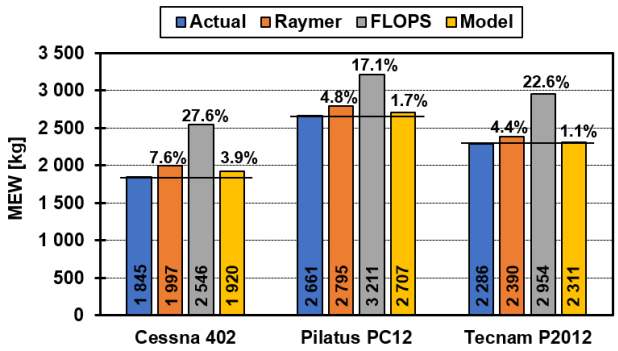

Figure 11: Comparison of weight deviations

The model shows great accuracy with respect to the MEW, as shown in Figure 11. The percentage values above the columns indicate the deviation from the actual weight. The high mean deviations of the FLOPS model are due to the highly overestimated system weight. This is verified by additionally comparing the weights with the calculated system weights of other models published in literature. A detailed mass breakdown of the *aDEPt* based on the developed model can be found in Table 5.

Description	Mass [kg]
Structure	**973**
Wing	291
V-Tail	61
Fuselage	432
Landing Gear	159
Nacelle	30
Propulsion	**748**
Turboshaft(installed)	239
Electrical components	393
Propeller	75
Fuel System	41
Systems	**403**
MEW	**2 124**
Battery	788
Fuel	379
Max. Payload	1 058
MTOW	**4 349**

Table 5: Mass breakdown of the *aDEPt*

The structural component weight is determined using empirical formulas based on FLOPS as it allows some additional refinements over the equations given by Raymer. To take the cargo loading system into account, the fuselage weight is calculated with the specific formula for transport fuselages. Moreover, the wing weight is calculated using the refined wing model for composite structures [28]. In order to consider the influence of composite on all other structural components, the corresponding factors proposed by Raymer are used [27].

The weight of the individual components of the hybrid-electric powertrain are calculated based on specific power ratios [15].

In order to ensure sufficient stability and controllability, a static margin of 10% is taken into account during the calculation of the *Center of Gravity* (CG). The whole problem is solved iteratively as CG-, mass-, landing gear and stability analysis influence each other.

4. PERFORMANCE ANALYSIS

This chapter discusses the aircraft performance with focus on T/O, landing, noise and cruise performance. To determine the overall performance of the aircraft, the wing including nacelles and the influence of the HLPs as well as the fuselage are simulated in *OpenFOAM*. The CFD model of the wing is validated against Stoll's momentum theory-based approximation as described in section 3.4.2. Subsequently, the individual aerodynamic components of the aircraft are assembled in accordance to Gudmundsson [8]. An overview of the *aDEPt's* key parameters resulting from the sizing process is shown in Table 6.

Parameter	Unit	Value
MTOW	[kg]	4 349
Battery mass	[kg]	787.68
Fuel tank	[l]	550
PAX	[-]	9
T/O-Distance	[m]	158.99
Landing distance	[m]	158.84
Cruise speed (max.)	[kts]	250
Stall speed	[kts]	49
Noise*	[dB]	64.35
Max range	[NM]	350
Electrical range	[NM]	125+
Length	[m]	12.0
Span	[m]	19.92
AR	[-]	15

* at flyover point

Table 6: Summary of key parameters

4.1. Take-Off and Landing

T/O is calculated by solving the equation of motion as proposed by Gudmundsson [8]. For T/O a flap setting of 20° as well as maximum thrust of the HLPs and CPs is considered leading to a mean acceleration of more than 5 m/s^2. This

enables a very short ground run of 65 m and allows the *aDEPt* to overfly a height of 35 ft within 158.99 m. For landing, flaps are at their full setting (40°), while the HLPs are at full thrust to enable the low stalling speed of 25 m/s. To keep the velocity constant the CPs already provide reverse thrust in the last segment of the final approach. As soon as the airplane touches down, the flaps move up to 9° to create downforce, while the CPs deliver maximum reverse thrust. This configuration yields a total landing distance of 158.84 m.

4.2. Noise

The *aDEPt* features low noise emissions underlined by stowing the TG in the aft as well as the DEP design approach. The latter significantly reduces engine noise. In order to estimate aircraft noise, the individual noise contributions from the most crucial components propeller, fuselage and wing are calculated individually. To predict the far-field propeller noise, a semi-empirical approach according to Marte et. al. is used [29]. Based on the motor power, a reference *Sound Pressure Level* (SPL) is determined for each drive. This SPL is then corrected by the number of blades, rotational speed, directional characteristics and attenuation due to spherical sound propagation. Selfridge et. al. has proposed an equation that can be used to calculate the harmonic distribution of sound up to the 10th order [30]. Depending on the loading sound frequency this leads to ten different SPL's which have to be corrected for atmospheric absorption.

The airframe noise is determined using the approximation proposed by Gibson [31]. As specified in procedure 24 CFR Part 36 Appendix G two SPLs are calculated at the relevant flyover points in segment one and two (see Table 7). This results in a peak SPL of 64.35 dB.

SPL [dB]	Segment 1	Segment 2
Propeller	50.74	62.70
Airframe	42.20	59.34
Aircraft	51.31	64.35

Table 7: SPL at segment one and two

4.3. Cruise Performance

The *aDEPt* uses multiple systems to enhance cruise performance and therefore reduce the impact of the additional battery weight on energy consumption. This allows efficient cruise operations at up to 250 KTAS, which is shown in Figure 12 in terms of L/D and electrical range as a function of cruise speed. The given electrical range incorporates a 10% battery power reserve for safety purposes.

With the majority of today's commuter flights being performed by aircraft restricted to a cruise speed of about 200 kts [5], the *aDEPt* excels in comparison with an *L/D* of 23.9 and an electrical range of 163 NM. This range would cover about 90% of CA's currently flown missions (see Figure 1). Furthermore, a total range of 280 NM can be achieved within the specified time span of 99 min with

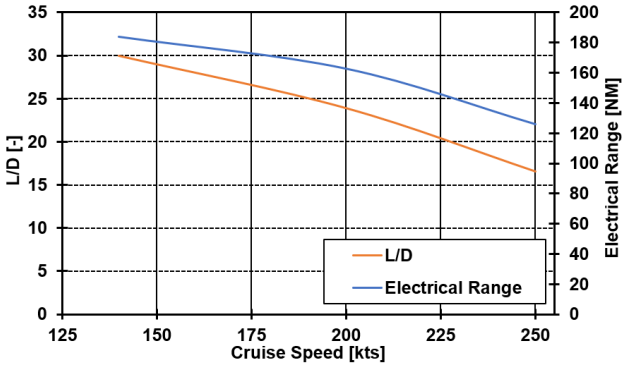

Figure 12: Cruise speed performance

the implementation of the TG. This flight mission consumes only 43.5 kg of fuel.

5. OPERATION CONCEPT

Because of its *Short T/O and Landing* (STOL) abilities and avionic equipment the *aDEPt* can service almost every airport worldwide only restricted by its span of 19.92 m. Airlines can therefore use more than 18 000 airports in the USA alone to build an air transport network that provides air services to remote areas [3]. To use the *aDEPt's* electrical capabilities, facilities for the recharge and/or swap of battery packs are needed. The ongoing research and support in electrical ground transportation, however, will benefit the integration of the majority of these airports into the electrical transportation network. This applies in particular to future small airparks, that might emerge in otherwise dense suburban areas.

The research conducted indicates that demand for thin-haul flights will increase significantly in the future, if OC fall to a certain level [32, 33, 6]. This opens up the possibility for operation concepts like the one depicted in Figure 13, which is based on the given design mission (see Table 8). This operation concept focuses on the maximum number of flights during a 18 hour utilization period. Taking the given turnaround and mission requirements into account, the *aDEPt* can fly up to 8 passenger and 4 cargo missions within the given 18 hour time frame.

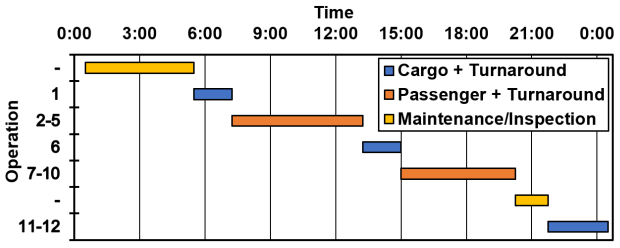

Figure 13: Gantt chart of the exemplary operation concept

Because of its cargo loading concept, the *aDEPt* can start with a piloted cargo mission early in the morning (5:30), outside of passenger rush hours. After delivery, the floorboards and seats are easily folded back into passenger configura-

tion during the scheduled turnaround. Subsequently, passengers who seek connection to the next major city can be conveniently transported. In order to avoid any downtime outside of passenger rush hours, an additional cargo mission can be flown in between passenger missions. At night the *aDEPt* undergoes light maintenance/inspections which includes the check of functionality of the TG and batteries as well as virtual tests of the autonomous system. This can be done within 90 min (including turnaround), which is enough time to fully charge the batteries considering the power output of current charging units. Since autonomous cargo missions neither require a pilot nor include the transportation of passengers, physiological constraints pertaining thereto are lifted. Thus these missions can be flown at a steeper climb rate as well as at an higher altitude to reduce noise and avoid icing conditions.

6. COST ESTIMATION

The Tecnam P2012, Cessna 402 and Pilatus PC12 are used as reference aircraft and compared to the *aDEPt* on basis of the design mission presented in Table 8 [34, 35, 36].

Parameter	Unit	Value
Range (complete)	[NM]	120
Range (electrical)	[NM]	120
Flight time	[min]	45*/60**
Turnaround	[min]	45*/30**
Passenger missions/day	[-]	8
Cargo missions/day	[-]	4
workload days/year	[-]	300

*passenger ** cargo

Table 8: Design mission

To account for inflation, all costs are adjusted to 2018-USD using the corresponding *Consumer Price Index* (CPI).

6.1. Acquisition Costs

The Eastlake business model, as proposed by Gudmundsson, is used to calculate the acquisition costs of the aircraft [8]. The wrap values recommended by Gudmundsson are inflation-adjusted to \$100, \$66 and \$58 per hour for engineering, tooling, and manufacturing, respectively. To calculate the electrical powertrain components the cost values proposed by Stoll are used [12]. Nykvist and Nilsson propose Battery costs of \$100/kWh to \$150/kWh for the year 2025 [37]. The upper bound of \$150/kWh is set as a conservative projection.

The resulting *List Price* (LP) amounts to **\$3 258 056** for a profit margin of 15%. This places the *aDEPt* between the P2012 (\$2.7M) and the PC12 (\$4.963M). This is reasonable, since the cost model shows the greatest sensivity in terms of structural weight and maximum airspeed, both of which are parameters where the *aDEPt* is closer to the P2012 than the PC12. The increased costs in relation to the P2012 are primarily due to composite structures and the additional avionics and powertrain costs.

6.2. Cash Flow Analysis

To reflect the profitability of the aircraft program for the manufacturer, the *Net Present Value* (NPV) and *Break Even Point* (BEP) are determined. The NPV can be calculated with Equation 3 using the already calculated *Design and Developement Costs* (DDC), *Production Costs* (PC) and list price.

$$NPV = -\frac{DDC}{PR} + \sum_{t=1}^{T} \frac{LP - PC}{(1+i)^t} \tag{3}$$

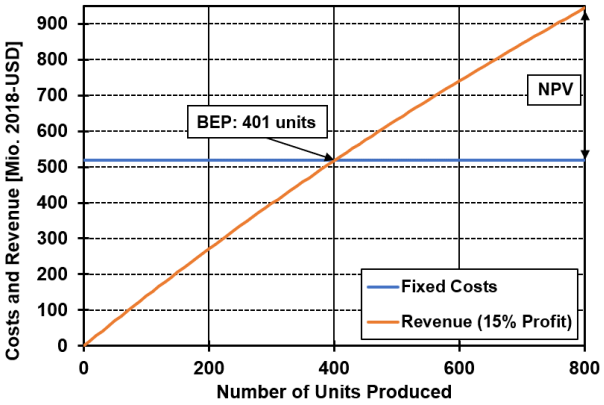

Figure 14: NPV and BEP for a 15% profit margin

The *Production Rate* (PR) is set to 800 aircraft over $T = 8$ years. To account for cash flow discounting an interest rate i of 5% is chosen. The NPV results in **\$422 251 831**. The BEP is reached at **401** aircraft sold as shown in Figure 14.

6.3. Operating Costs

To calculate the OC of the *aDEPt* the following must be considered:

- **Energy Costs** \$0.0692/kWh (average 2018 industrial rate) and a charger efficiency of 95%. \$4.5/gallon for 100LL fuel (for the reference aircraft) [14, 38].
- **Overhaul:** According to Harish, electric motors will not be overhauled during their operating life [39].
- **Maintenance:** Electric motors and composite airframes require less maintenance. Therefore discount factors are introduced and multiplied with the hourly maintenance cost rate of \$140 proposed by Stoll [12]. A cost reduction of 20% for electric motors and 35% for a composite airframe are proposed by literature [40, 41]. This results in a weighted cost rate of \$101.5/hour.
- **Labor:** \$40/hour [8]. Since the turnaround times are low, the rate is applied to the complete utilization period instead of just the block time.
- **Fees:** Calculated according to Gudmundsson [8].
- **Battery:** The batteries need to be replaced after 2 000 charging cycles for \$150/kWh [42, 37].
- **Storage:** \$18 000 [8].

- **Depreciation:** In addition to the aircraft, a charging station worth $300 000 is being depreciated over a period of 20 years [43].
- **Insurance:** Calculated according to Gudmundsson [8].
- **Interest:** 6% interest rate. It is conservatively assumed that the entire purchase price needs to be financed over a 10 year loan period.
- **Others:** Ticketing, administration, promotion costs, etc. are considered with a surcharge factor on costs-of-goods-sold (all OC except for capital expenditures) of 10% [14].

The cost model calculates the OC of the *aDEPt* to **$2.777/NM** ($336/flight, $0.309/ASM (*Available Seat Mile*), $454/flighthour) when operated by one pilot, making it 30.2%, 33.3% and 46.6% cheaper to operate than the P2012, C402 and PC12, respectively. Figure 15 shows the individual cost components of the *aDEPt* and the reference aircraft.

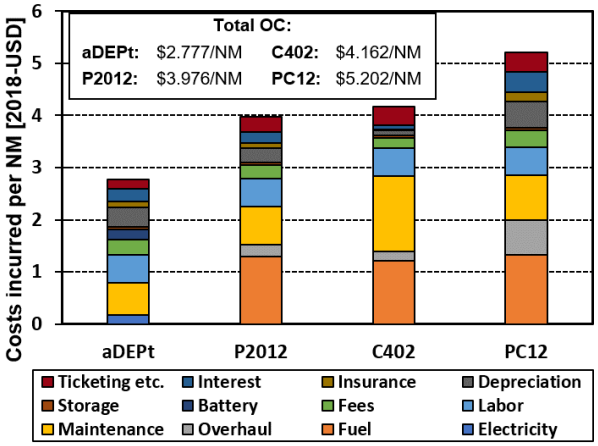

Figure 15: Operating cost estimates

Taking into account the purchase price, the *aDEPt* is therefore more profitable than the PC12 from the outset. Amortization in relation to P2012 is achieved after one operating year. The Cessna 402 is no longer produced and is hence not considered here.

6.4. Impact of Autonomy

In order to illustrate the influence of autonomous flights on costs, insurance and labor costs need to be examined. A *Ground Pilot* (GP) is needed for safety purposes [14, 12]. It is assumed that on average one GP can oversee five aircraft for the same cost rate of $40/h [14]. Furthermore, the GP will only monitor the aircraft for the duration of its block time. Additionally, it is assumed that insurance costs will initially rise for non-piloted aircraft due to the risk aversion of insurance groups. However, it is expected that autonomy will reduce the risk of accidents, as otherwise the technology will not be able to establish itself on the market. Therefore for a fully autonomous mission in a distant future instead of the FAR Part 23 rates the FAR Part 25 rates are applied, as the technology must already be well established on the market to ensure autonomous passenger transport. Figure 16 illustrates the effect of autonomy on the costs.

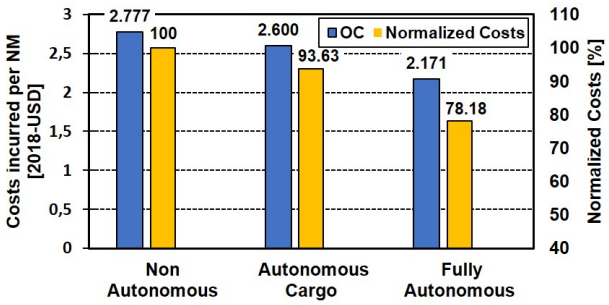

Figure 16: Impact of autonomy on costs

OC decrease by 6.37% if an autonomous cargo mission is taken into account. This leads to OC of $2.600/NM ($315/flight, $0.289/ASM, $425/flighthour). In case of fully autonomous operations, the OC decrease by 21.82%, leading to OC of $2.171/NM ($263/flight, $0.241/ASM, $355/flighthour).

7. CONCLUSION

The *aDEPt* presents a versatile aircraft concept that offers an efficient and cost-effective transport model for connecting remote towns or small cities to larger central hubs in metropolitan areas. By combining a hybrid-electrical DEP approach with increased autonomy, the three biggest challenges of commuter airlines are addressed: high OC, lack of qualified pilots and demanding routes.

With its T/O and landing distance of just under 160 m the *aDEPt* can land at almost every airport in the world and enables compatibility with future small airparks emerging in suburban areas. This is complimented by the low noise level of 64.35 dB at the flyover point. In addition to the multi-redundant hybrid-electric DEP configuration, the dual cruise motor configuration and powertrain system architecture further decrease error-proneness. Additionally the *aDEPt's* avionic configuration allows for autonomous operations, making it a sustainable aircraft for the future.

Through the cabin conversion and loading concept, its electrical range of 125 NM at a maximum cruise speed of 250 kts, as well as the maximum range of 350 NM (within 99 min), the *aDEPt* provides numerous operational possibilities. In combination with the high *W/S* and the morphed TE the *aDEPt* further offers a smooth, gust insensitive, flight feeling and at the same time increases cruise performance significantly. This is especially evident in the high *L/D* of 23.9 at a typical commuter aircraft cruise speed of 200 kts.

The combination of its key technologies ultimately makes the *aDEPt* less expensive to operate than its direct competitors. In comparison with the P2012, C402 and PC12, initial calculations show savings in OC of 30.2%, 33.3% and 46.6%, respectively, when operated by one pilot. This advantage further increases to 34.6%, 37.5% and 50.0%, respectively, if cargo missions are flown autonomously and 45.4%, 47.8% and 58.3%, respectively, if all missions are flown autonomously.

References

[1] A. Metrass-Mendes, R. Neufville, and A. Costa, "Air accessibility in northern canada; prospects and lessons for remote communities."

[2] United Nations Department of Economic and Social Affairs, "World urbanization prospects, 2014 revision," *US Air Force Wright Lab., Wright–Patterson AFB, OH, Rept. WL-TR-93-3082*, 2014.

[3] S. A. Viken, F. M. Brooks, and S. C. Johnson, "Overview of the small aircraft transportation system project four enabling operating capabilities."

[4] F. Wei and T. H. Grubesic, "A typology of rural airports in the united states: Evaluating network accessibility," in *The Review of Regional Studies*, Southern Regional Science Association, Ed., 2015.

[5] D. Wolf and L. Markham, "Commuter airline persepctive: On-demand mobility and follow up workshop," 08.03.2016.

[6] D. A. Wolf, "Air service to small and rural communities."

[7] N. Arnhem, T. Sinnige, T. C. Stokkermans, G. Eitelberg, and L. L. Veldhuis, "Aerodynamic interaction effects of tip-mounted propellers installed on the horizontal tailplane," in *2018 AIAA Aerospace Sciences Meeting*. Reston, Virginia: American Institute of Aeronautics and Astronautics, 01082018.

[8] S. Gudmundsson, *General Aviation Aircraft Design: Applied Methods and Procedures*. Elsevier Inc., 2014.

[9] Patterson M. D., "Conceptual design of high lift propeller systems for small electric aicraft," Dissertation, Georgia Institute of Technology, 2016.

[10] M. D. Patterson and N. K. Borer, "Approach considerations in aircraft with high-lift propeller systems," in *17th AIAA Aviation Technology, Integration, and Operations Conference*. Reston, Virginia: American Institute of Aeronautics and Astronautics, 06052017.

[11] N. K. Borer, M. D. Patterson, J. K. Viken, M. D. Moore, S. Clarke, M. E. Redifer, R. J. Christie, A. M. Stoll, A. Dubois, J. Bevirt, A. R. Gibson, J. F. Foster, and P. G. Osterkamp, "Design and performance of the nasa sceptor distributed electric propulsion flight demonstrator."

[12] A. M. Stoll and G. V. Mikic, "Design studies of thin-haul commuter aircraft with distributed electric propulsion," in *16th AIAA Aviation Technology, Integration, and Operations Conference*. Reston, Virginia: American Institute of Aeronautics and Astronautics, 06132016.

[13] F. Settele and A. Knoll, "Untersuchung der flugleistung eines elektroflugzeuges mit einem neuartigen elektromotor," *Deutscher Luft- und Raumfahrtkongress*, 2015.

[14] M. Kreimeier, "Evaluation of on-demand air mobility concepts with utilization of electric powered small aircraft," Dissertation, RWTH Aachen, 2018.

[15] R. Jansen, C. Bowman, and A. Jankovsky, "Sizing power components of an electrically driven tail cone thruster and a range extender," in *16th AIAA Aviation Technology, Integration, and Operations Conference*. Reston, Virginia: American Institute of Aeronautics and Astronautics, 06132016.

[16] S. Coulsdon, *IHS Jane's Aero-Engines*. IHS Global Limited, 2014.

[17] N. Aminian and F. Romli, "Ergonomics assessment of current aircraft passenger seat design against malaysian anthropometry data," *International Journal of Engineering & Technology*, vol. 7, no. 4.13, p. 18, 2018.

[18] J. Porta, G. Saco-Ledo, and M. Cabanas, "The ergonomics of airplane seats: The problem with economy class," *International Journal of Industrial Ergonomics*, vol. 69, pp. 90–95, 2019.

[19] IOS, "Flat pallets for intercontinental materials handling – principal dimensions and tolerances: Standard," Geneva, CH.

[20] G. Raballand and E. Aldaz-Carroll, "How do differing standards increase trade costs? the case of palletts," *The World Bank*, no. World Bank Policy Research Working Paper 3519, 2005.

[21] Sea Air Transport & Service, "Was bedeutet der begriff volumengewicht/chargeable weight?" 2019. [Online]. Available: https://www.sats-logistics.com/glossar/volumengewicht-chargeable-weight/

[22] Wolfgang Kempkens, "Nasa experimentiert mit flexiblen hinterkanten." [Online]. Available: https://www.ingenieur.de/technik/fachbereiche/raumfahrt/dehnbare-huelle-laerm-wirbel-an-tragflaechen-senken/

[23] E. Stumpf, "Flugzeugbau ii ; stabilität und steuerbarkeit," 2019.

[24] M. Drela and H. Youngren, "Xfoil: Subsonic airfoil development system." [Online]. Available: https://web.mit.edu/drela/Public/web/xfoil/

[25] P. E. Purser and J. P. Campbell, "Experimental verification of a simplified vee-tail theory and analysis of available data on complete models with vee tails."

[26] D. Moormann, "Flugdynamik;," 2019.

[27] D. P. Raymer, *Aircraft Design: A Conceptual Approach*. Washington D.C.: American Institute of Aeronautics and Astronautics, 2006.

[28] D. P. Wells, B. L. Horvath, and L. A. McCullers, "The flight optimization system weights estimation method."

[29] J. F. Marte and D. E. Kurtz, "A review of aerodynamic noise from propellers, rotors and lift fans."

[30] R. Selfridge, D. Moffat, and J. D. Reiss, "Physically derived sound synthesis model of a propeller," *ACM*, 2017.

[31] J. S. Gibson, “Non-engine aerodynamic noise investigation of a large aircraft.”

[32] S. Roy, A. Maheshwari, W. A. Crossley, and D. A. DeLaurentis, “A study on the impact of aircraft technology on the future of regional transportation using small aircraft,” in *2018 Aviation Technology, Integration, and Operations Conference*. Reston, Virginia: American Institute of Aeronautics and Astronautics, 06252018, p. 13.

[33] J. C. Smith, J. K. Viken, N. M. Huerreiro, S. M. Dollyhigh, J. W. Fenbert, C. L. Hartmann, T.-S. Kwa, and M. D. Moore, “Projected demand and potential impacts to the national airspace system of autonomous, electric, on-demand small aircraft,” in *12th AIAA Aviation Technology, Integration, and Operations (ATIO) Conference and 14th AIAA/ISSMO Multidisciplinary Analysis and Optimization Conference*. Reston, Virigina: American Institute of Aeronautics and Astronautics, 09172012.

[34] Cape Air, “Cessna 402c limitations/systems review guide.”

[35] Pilatus Aircraft Ltd, “Pc-12 ng just the facts,” 2016.

[36] TECNAM, “P2012 traveller,” 2017.

[37] B. Nykvist and M. Nilsson, “Rapidly falling costs of battery packs for electric vehicles,” in *Nature Climate Change*, 2015, pp. 329–332.

[38] Rocky Mountain Power, “Industrial price comparison,” 2019. [Online]. Available: https://www.rockymountainpower.net/about/rar/ipc.html

[39] A. Harish, C. Perron, D. Bavaro, J. Ahuja, M. Ozcan, C. Y. Justin, S. I. Briceno, B. J. German, and D. Mavris, “Economics of advanced thin-haul concepts and operations,” in *16th AIAA Aviation Technology, Integration, and Operations Conference*. Reston, Virginia: American Institute of Aeronautics and Astronautics, 06132016, p. 1.

[40] Boeing, “Boeing 787: From the ground up.”

[41] B. Propfe, M. Redelbach, D. J. Santini, H. Friedrich, and S. Mercedes, “Cost analysis of plug-in hybrid electrical vehicles including maintenance & repair,” in *EVS26 International Battery, Hybrid and Fuel Cell Electric Vehicle Symposium*, 2012.

[42] B. Diouf and R. Pode, “Potential of lithium-ion batteries in renewable energy,” in *Renewable Energy*, 2015, pp. 375–380.

[43] ARK Invest, “Supercharger: A charge could cost half the price of gas,” 2016. [Online]. Available: https://ark-invest.com/research/supercharger-cost-comparison#fn-6240-2

Appendix

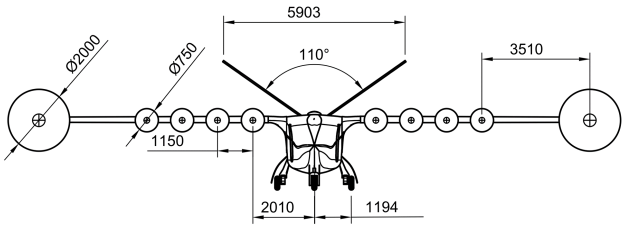

Figure 17: Front view of the *aDEPt*

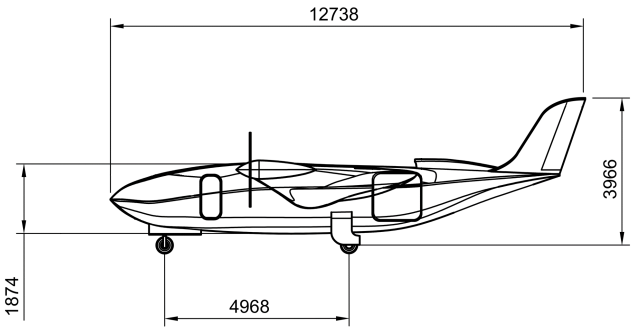

Figure 18: Side view of the *aDEPt*

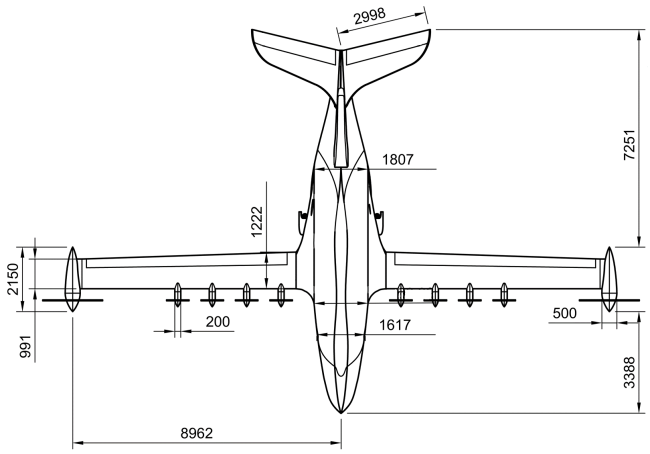

Figure 19: Top view of the *aDEPt*

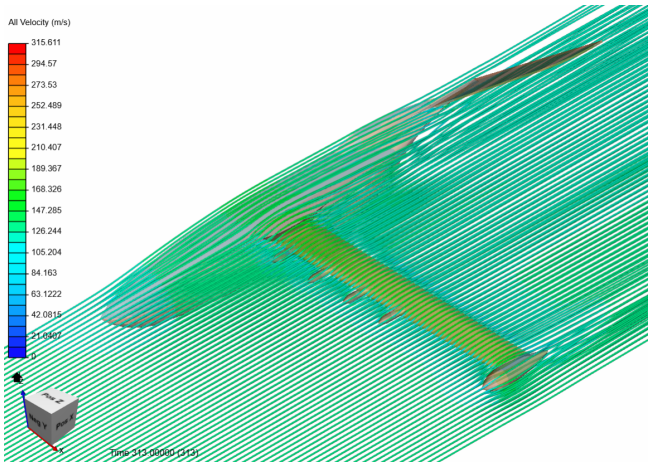

Figure 20: OpenFOAM velocity simulation